Title

Evaluation of simulated ground motions using probabilistic seismic demand analysis: CyberShake (ver. 15.12) simulations for Ordinary Standard Bridges

Authors

Fayaz, Jawad
Rezaeian, Sanaz
Zareian, Farzin

Publication Date

2021-02-01

DOI

10.1016/j.soildyn.2020.106533

Peer reviewed

Soil Dynamics and Earthquake Engineering 141 (2021) 106533

Contents lists available at ScienceDirect

Soil Dynamics and Earthquake Engineering

journal homepage: http://www.elsevier.com/locate/soildyn

Evaluation of simulated ground motions using probabilistic seismic demand analysis: CyberShake (ver. 15.12) simulations for Ordinary Standard Bridges

Jawad Fayaz [a], Sanaz Rezaeian [b], Farzin Zareian [a,*]

[a] Department of Civil and Environmental Engineering, University of California, Irvine, CA, USA
[b] U.S. Geological Survey, Golden, CO, USA

ARTICLE INFO

Keywords:
Simulated ground motions
CyberShake
Ordinary bridges
Validations

ABSTRACT

There is a need for benchmarking and validating simulated ground motions in order for them to be utilized by the engineering community. Such validation may be geared towards a specific ground motion simulation method, a target engineering application, and a specific location; the validation presented herein focuses on a bridge engineering application in southern California. Catalogs of simulated ground motions representing a 200,000-year forecast are selected from the Southern California Earthquake Center CyberShake version 15.12 database for five sites in Southern California (~20,000 unscaled ground motions per site). They are used in Non-Linear Time History Analysis (NLTHA) of four Ordinary Standard Bridge structures. For each site, these data are used to obtain simulation-based Engineering Demand Parameter (EDP) hazard curves. These are compared against EDP hazard curves that are constructed using conventional methods based on empirical models, i.e., using recorded ground motions through Incremental Dynamic Analysis and integration over the Intensity Measure (IM) hazard curve. The two sets of simulation-based and conventional EDP hazard curves are compared at various return periods. To further account for the differences between simulated and recorded ground motions, direct comparisons are also made between IM hazard curves for simulated and recorded catalogs, as well as the EDP versus IM data obtained from NLTHA of the bridges. We observe that CyberShake simulates motions that yield similar EDP values compared to empirical data for shorter return periods. For longer return periods, however, EDPs from the simulation-based analysis tend to be lower than the EDPs obtained from utilizing recorded ground motions for short-period bridges, while the opposite is the case for long-period bridges. It is recommended that validation efforts go beyond IM levels and also include comparisons of the relations between IMs and EDPs. Finally, site-specific relations are proposed that correlate the ratio between the two types of EDPs (simulation-based and conventional) with the hazard level, shallow site condition, and site basin depth.

1. Introduction

A typical assumption in engineering of critical structures and infrastructure for seismic hazard is approximating possible seismic excitations during the expected lifetime of the structure by selecting and modifying a set of ground motion time-series from recordings of past events world-wide [1]. This recorded set of ground motions is used for Non-Linear Time History Analysis (NLTHA) to obtain the structural response. The process by which recorded ground motions are selected and modified is a significant branch of earthquake engineering research and has led to recommendations on how to use a multitude of target design response spectra for this process. Design response spectra representing the target seismic hazard at a specific site were stipulated in ASCE 7–05 [2]; uniform-hazard spectra have been recommended by Pacific Earthquake Engineering Research (PEER) Tall Buildings Initiative (TBI) [3]; and conditional mean spectra are specified in ASCE 7–16 [4]. All three require selecting ground motions that match the dominant event parameters (e.g., magnitude, source-to-site distance) for the design hazard level and local soil conditions. The fundamental assumption that recordings from past world-wide earthquakes can be used for engineering of new structures in locations with different seismic characteristics has several limitations. These limitations include bias in the estimation of structural response when using different ground motion selection and modification methods (e.g., [5,6]), and gaps in

* Corresponding author.
E-mail address: zareian@uci.edu (F. Zareian).

https://doi.org/10.1016/j.soildyn.2020.106533
Received 28 July 2020; Received in revised form 5 November 2020; Accepted 1 December 2020
Available online 30 December 2020

recorded ground motion databases for large-magnitude events at short source-to-site distances (e.g., [7]). Using simulated ground motions can overcome these limitations, and recently the methods and required infrastructure to simulate ground motions have significantly improved (e.g., [8–11]). Due to such advancements in simulations, much attention has been given to validation research in recent years (e.g., [7,12–19,44]). The engineering community is gradually moving towards embracing simulated ground motions in practice (e.g., [20–23]). The study presented herein is a move in the direction of validating and utilizing simulated ground motions for bridge engineering practice.

Current bridge design practice is based on utilizing design acceleration response spectra with an approximately 7% probability of occurrence in 75 years. When using NLTHA for assessing the behavior of bridge structures, engineers select ground motion records and adjust them to the desired desing spectrum using linear scaling or spectral matching methods. Such an approach can be improved to (1) directly incorporate near-field effects such as directivity and directionality, (2) more accurately represent ground motion time-domain characteristics such as strong motion duration and velocity pulses that could be distorted in the scaling and spectral matching routines, and (3) provide direct matching of two orthogonal components of ground motions in the proposed adjustments. These and other improvements can be achieved by utilizing synthetic ground motions generated from physics-based simulation methods (e.g., the Southern California Earthquake Center's CyberShake and Broadband simulation platforms, [10,26,46]). In other words, some of the challenges that engineers face in the selection and scaling/modification methods of recorded ground motions for Performance Based Earthquake Engineering (PBEE) of the Ordinary Standard Bridges (OSBs) can be overcome by utilizing simulated ground motions that are tailored for a target location. The research work summarized herein is a step in harnessing the capabilities of synthetic ground motions for design and assessment of OSBs based on PBEE concepts and in an applied and standardized format.

A significant challenge in validating simulated ground motions is the diversity of engineering applications, validation methods, and the lack of consensus on the acceptable accuracy for estimating structural response if simulated motions are utilized. Recent validation efforts have focused on using historical events as the bases of comparison (e.g., [7,13,16,19,44]). Such an approach (denoted here as Type I Validation) would show if ground motion simulation methods can generate waveforms of past events that affect structures in the same way–statistically–that the natural recordings of the same events do. Type I Validation can be exercised for significant ground motion Intensity Measures (IM) (e.g., peak ground acceleration, spectral acceleration at various periods, the ratio of maximum to median spectral displacement demand) or structural response parameters (a.k.a. Engineering Demand Parameters, EDPs). Validation strategies have evolved to Type II Validation methods in which the variation of IMs (or EDPs) with event parameters is investigated (e.g., [12,15]. The closeness in the trends with event parameters between simulated and recorded ground motions is used as a measure to validate a simulation method. Type III Validation has been suggested to facilitate the use of simulated ground motions as a database of time series (similar to the database of NGA-West2 records; [45]) from which engineers can select and modify time series for design codes and guidelines (e.g., ASCE 7–16, 2017; FEMA P-58, 2018; PEER [3]; and [24]. In Type III Validation, a ground motion simulation method is judged by the similarity of structural response statistical parameters obtained from sets of simulated and recorded motions anchored to a given target response spectrum (e.g., [17,25].

The study presented herein focuses on probabilistic seismic demand analysis of structures conducted with simulated and recorded motions. The evaluation is for bridge engineering applications and CyberShake [26] version 15.12 simulations. For five sites located in Southern California with diverse site and local seismicity conditions, catalogs of simulated ground motions representing 200,000 years are obtained from the CyberShake database. CyberShake [26] is a ground motion simulation tool that contains ground-motion waveforms representing scenarios present in the Uniform California Earthquake Rupture Forecast, Version 2 (UCERF2) [27] in Southern California. At each site, the selected catalog contains roughly 20,000 ground motions from events with $M_w > 6.0$ occurring within a vicinity of 200 km. For each site, the catalog of simulated ground motions is applied to four OSBs in NLTHA. To consider the possibility of bridges being placed at an angle to the simulated ground motions, the ground motions are rotated in 10° increments and applied to the bridge models (i.e., 18 rotations for each ground motion spaning 0° to 180°). For each combination of bridge and site, column drift demands obtained from NLTHA data are used to generate EDP hazard curves. These data are compared with the results obtained from conventional methods where recorded ground motions are used to conduct Incremental Dynamic Analysis (IDA) of the bridge and the results are integrated over a ground motion IM hazard curve for the site. A comparison between the two methods for obtaining column drift ratios at various hazard levels informs how simulated ground motions from CyberShake can be utilized for bridge engineering practice. Finally, site-specific predictive relations are proposed that correlate the ratio between the two types of EDPs with hazard level, shallow site condition, and site basin depth. The proposed relations can assist engineers to scale the EDPs as per the effects of site and basin conditions.

2. Ground motion database

This study uses the ground motions simulated for CyberShake [26] version 15.12 from the Southern California Earthquake Center (SCEC). CyberShake [26] is a computational platform that integrates a collection of scientific software and middleware to perform 3D physics-based simulations. For the CyberShake 15.12 study, deterministic source-based (physics-based) models are utilized in simulations for frequencies up to 1 Hz; the results are then augmented with high-frequency (1–10 Hz) stochastically simulated seismograms produced using the Graves and Pitarka [10] module from the SCEC Broadband platform [46]. The study simulated ground motions for 337 sites on a closely-spaced grid in the Southern California region. Among these, a subset of five representative sites is selected for the research conducted in this paper. The selected sites include Los Angeles downtown (LADT), San Bernardino strong motion (SBSM), 710-91 Interchange (STNI), Whittier Narrows Golf Course (WNGC), and Century City Plaza (CCP) sites. The sites LADT and CCP are located within the northern Los Angeles basin and are selected because of their proximity to a large inventory of buildings and bridge structures of societal importance. STNI is situated on a very deep part of the basin in this region, where the effects of the geologic basin on the resulting ground motions are highly pronounced [26]. The WNGC and SBSM sites are interesting because they exhibit coupling of basin and directivity effects in the ground motions [26]. Fig. 1 shows the locations of the selected five sites in the Southern California region.

The earthquake rupture forecast used in the CyberShake 15.12 study is based on the UCERF2 single branch model [27]. However, it does not use UCERF2 directly and performs some modifications and incorporates additional constraints. These modifications include setting the minimum magnitude of considered earthquakes to 6, excluding background seismicity, and adjusting rupture areas for consistency with the simulation model [26]. For each site, CyberShake-UCERF2 provides a list of potential ruptures with their annual probabilities of occurrences and also introduces a suite of variations in the hypocenter location and slip distribution to account for the natural variability in rupture characteristics. This process results in an average of 415,000 rupture variations for each site. Each rupture variation is associated with a ground motion waveform simulated for the CyberShake 15.12 study. The ruptures are assumed to be independent and all the hypocentral variations are assumed to be equally likely for each rupture. For the selected subset of five sites, Monte Carlo simulations are used to obtain a catalog of ground motion simulations representing a 200,000-year forecast within 200 km

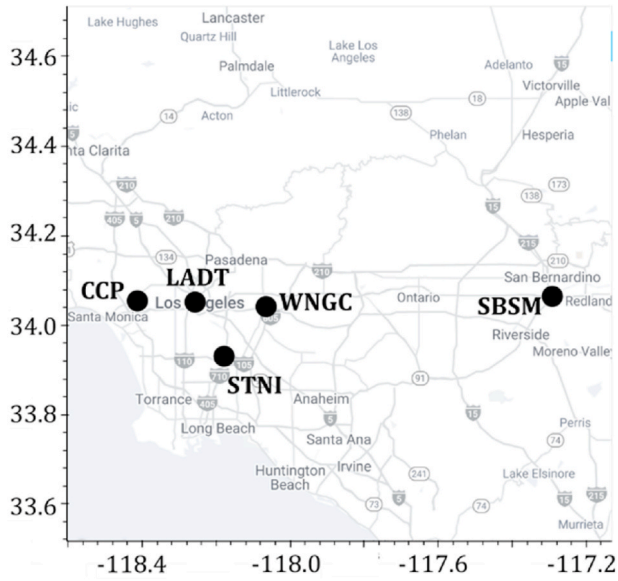

Fig. 1. The selected subset of five sites in the greater Southern California region.

of the site. This is done by randomly sampling rupture variations for each site according to their annual probabilities of occurrences and then obtaining their corresponding ground motions. The obtained catalog represents a realization of ~20,000 ground motions that may occur at the site over 200,000 years. Table 1 includes the site information and the number of events (or ground motions, GMs) in the simulated catalog for each site. The site information includes shear-wave velocity averaged over the top-most 30 m of soil (V_{s30}), and the depth where shear-wave velocity is equal to 2.5 km/s ($Z_{2.5}$) (a.k.a. basin depth) obtained from Lee et al. [28]. Table 1 also provides information about the number of ground motions classified as pulse-like among the simulated catalogs using the algorithm proposed by Shahi and Baker [29].

3. Ordinary Standard Bridge structure models

This study is focused on four California Department of Transportation (Caltrans) OSBs. Four Reinforced Concrete ordinary symmetric bridge structures are selected as representatives for the statistical analysis. Table 2 includes the details of the four OSBs with seat-type abutments, which reflect the common bridge engineering practice in California. The first selected bridge is the *Jack Tone Road Overcrossing* (Bridge A) located in the city of Ripon, with two symmetric spans supported on a single column. The second bridge is the *La Veta Avenue Overcrossing* (Bridge B) located in the city of Tustin, with two symmetric spans supported on a two-column bridge bent. The third bridge is the *Jack Tone Road Overhead* (Bridge C) located in Ripon, with three symmetric spans and two three-column bridge bents. The fourth bridge is the curved *E22-N55 Connector Over-crossing* (Bridge F) located in Santa Ana, with four symmetric spans supported on single columns.

Finite Element models of these bridge structures are developed using

Table 2
Characteristics of bridge structures.

Bridge	A	B	C	F
Name	Jack Tone Road Overcrossing	La Veta Avenue Overcrossing	Jack Tone Road Overhead	E22-N55 Connector Over-crossing
Total Length	220.6 ft	300.0 ft	418.0 ft	500.0 ft
Number of Spans	2	2	3	4
Column Bent	Single-column	Two-column	Three-column	Single-column
Column Radius	33.1 in	33.5 in	33.1 in	47.7 in
Column Height	22.0 ft	22.0 ft	24.1 ft	18.5 ft
Reinforcement of Column Section	Long: 44 #11 (bundles of 2) Trans: Spiral, #6 @ 3.34 in	Long: 44 #11 (bundles of 2) Trans: Spiral, #4 @ 6.00 in	Long: 34 #14 (bundles of 2) Trans: Spiral, #7 @ 4.52 in	Long: 42 #14 (bundles of 2) Trans: Spiral, #7 @ 2.95 in
1st Mode Period (T^*)	0.61 s	0.82 s	0.78 s	1.11 s
2nd Mode Period	0.41 s	0.48 s	0.44 s	0.54 s

OpenSees [30]. The models are developed to represent the geometry, boundary conditions, mass distribution, energy dissipation, and the interaction between elements. Since many components of each bridge exhibit nonlinear behavior during seismic events, a fully 3D nonlinear model is developed by appropriately combining the components. The model comprises seat-type abutments (which include an arrangement of springs for shear keys, elastomeric bearing pads, backfill soil, and abutment piles), column bents (which include nonlinear fiber sectional models for columns and column foundational springs), and an elastic superstructure representing the deck. Detailed representation of the OpenSees models of these bridge structures is given in Fig. 2a. The model elements are briefly described below; see Fayaz et al. [23] for in-depth details of the modeling strategy.

The Caltrans Seismic Design Criteria (Caltrans SDC; 2013 and 2019) recommend that the superstructure be designed to remain elastic during an earthquake event; therefore, the superstructure is modeled with the elasticBeamColumn element of OpenSees using uncracked section properties. The mass of the superstructure is distributed throughout the length of the deck, with each span's mass being distributed in 10 intervals. The bridge columns are modeled using the beamWithHinges element (two Gauss integration points) with fiber-discretized cross sections. This is done to separately model confined concrete for the core, unconfined concrete for the cover, and steel rebars. The plasticity in the columns is concentrated at two plastic hinges located at the opposite ends of the columns connected by a linear elastic element. The plastic hinge length is determined based on the Caltrans SDC [31,32]. The hysteretic behavior of the columns is presented in Fig. 2f. Assuming monolithic construction of cap beams and columns, the cap beam is modeled as a rigid bent using the elasticBeamColumn element with high torsional, in-plane, and out-of-plane stiffnesses. The concrete and steel are modeled using the Concrete01 and ReinforcingSteel materials, respectively, available in OpenSees.

The bases of Bridge A and Bridge F are simulated as fixed

Table 1
Site characteristics and number of ground motions in simulated earthquake catalogs.

Site	V_{s30} (m/s)(CVM 4.26)	$Z_{2.5}$ (km)(CVM 4.26)	Location		No. of GMs in 200,000-year catalog	No. of Pulse-Like GMs in 200,000-year catalog
			Latitude	Longitude		
LADT	358.6	2.08	34.052	−118.257	20,984	783
SBSM	354.8	1.77	34.064	−117.292	22,848	1721
CCP	361.7	2.96	34.054	−118.413	19,822	965
WNGC	295.9	2.44	34.041	−118.065	21,359	1167
STNI	268.5	5.57	33.930	−118.179	20,415	1014

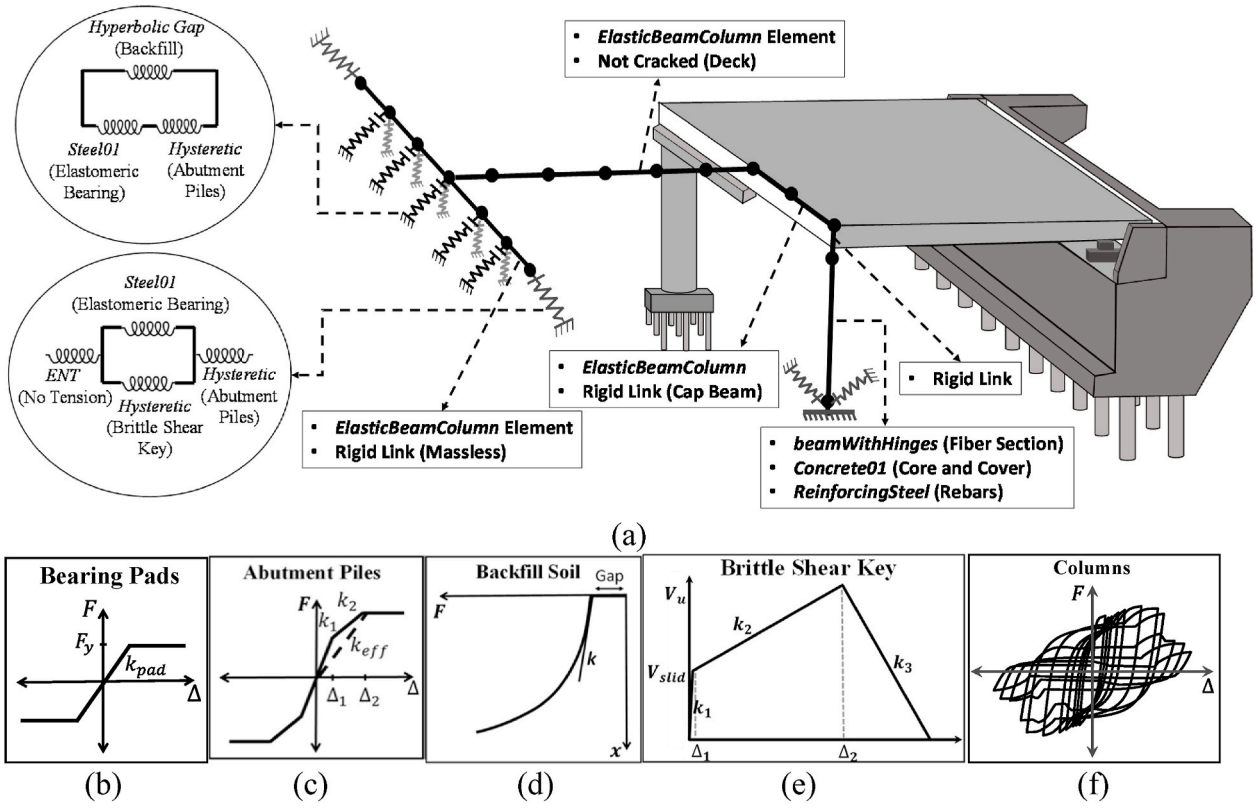

Fig. 2. a) Details of the finite-element model of bridges, b) bearing pads response, c) abutment pile response, d) backfill soil response, e) brittle shear key response, and f) column response.

connections, while the bases of Bridge B and Bridge C are simulated as pinned connections. However, the flexibility of base connections arising from piles beneath is modeled explicitly by describing the translational behavior of pile foundations using a linear elastic spring model, although vertical movement is restricted. For the transverse direction of the abutments, shear keys are designed and modeled to behave in a brittle/isolated manner, as per the experimental results of Kottari [33]. Shear keys are modeled using the hysteretic spring model available in OpenSees. The model is defined with a trilinear backbone curve, as given in Fig. 2e. The model of the abutment in the longitudinal direction comprises (i) abutment piles, (ii) backfill soil, and (iii) elastomeric bearing pads. Piles of the abutments are modeled through a trilinear hysteretic spring model in OpenSees with the backbone curve defined by Choi [34]. The backbone is presented in Fig. 2c. The backfill soil is modeled using the HyperbolicGapMaterial material with a Generalized Hyperbolic Force-Deformation (GHFD) backbone [35]. Fig. 2d shows a typical backfill force-displacement backbone curve. The piles underneath the abutment provide the active resistance of the abutment, while the combined action of the piles and backfill soil provides the passive resistance. The parameters described by Ramanathan [36] are used to model the elastomeric bearing pads with the Steel01 material. Fig. 2b shows the force deformation response of the elastomeric bearing pad. The longitudinal behavior of the abutment is modeled using five longitudinal abutment combo springs in parallel connected by a rigid link. In contrast, the transverse behavior is modeled using one combo spring at each end of the abutment (Fig. 2a).

4. Methodology for evaluating simulated ground motions

4.1. NLTHA using cybershake ground motions

The simulated ground motions for two orthogonal horizontal components are used to perform NLTHA of the four bridge structures at each site. Due to the significant difference in the dynamic characteristics of bridge structures in the two orthogonal directions, the bi-directional components of simulated ground motions are applied in incremental rotations from 0° to 180° (excluding 180° for straight bridges) with 10° increments. Hence, this study is based on the results of 5 sites × 20,000 ground motions × 4 bridges × 18 incidence angles = 7,200,000 NLTHA (360,000 NLTHA for each of the four bridges for every site). The behavior of OSB structures is mainly deduced by examining the maximum Column Drift Ratio (CDR) of the central bent throughout the time history of ground motion. Therefore, to be consistent with this practice and the ground motion intensity measure used, the EDP considered in this research is the median value of the maximum CDR obtained after applying the two components of ground motions at the 18 incidence angles. This EDP is denoted as *Rot50CDR*, where *Rot* indicates the rotation of ground motion components, 50 indicates the percentile of EDP used (among the 18 incidence angles), and *CDR* indicates Column Drift Ratio. The idea behind *Rot50CDR* is similar to the current state-of-practice IM *RotD50* spectral acceleration (S_a) [37]. *RotD50* S_a is an IM obtained after conducting elastic Linear Time-History Analysis (LTHA) on a single-degree-of-freedom (SDOF) oscillator; whereas *Rot50CDR* is a measure of the EDP obtained after conducting NLTHA on a multi-degree-of-freedom (MDOF) bridge model. In this study, for the sake of brevity, *RotD50* S_a is used interchangeably with S_a or $S_a(T)$. Hence, each ground motion is associated with one value of*RotD*50 $S_a(T)$ (as the IM) and one value of *Rot50CDR* (as the EDP).

The *Rot50CDR* and *RotD*50 $S_a(T)$values obtained from the catalogs of simulated ground motions are used directly to develop EDP and IM hazard curves, respectively. This is accomplished by sorting the ~20,000 EDPs and IMs in descending order and dividing their order number by the time span of 200,000 years to attain the average annual rate of exceedance of EDPs (λ_{EDP}) and IMs (λ_{IM}). Each *Rot50CDR* hazard curve obtained from this simulation-based analysis is termed as CS_{num}, an acronym for CyberShake Numeric. It should be noted that the

simulated catalogs not only represent the uncertainty in $S_a(T)$ for 200,000 years, but also represent the variability in other ground motion characteristics such as Arias intensity, duration, and frequency content. Hence, even for similar levels of $S_a(T)$, variability in all these ground motion characteristics can lead to variability in the response of the structures.

4.2. Selection of recorded ground motions for IDA

The data obtained from conducting NLTHA using CyberShake ground motions are compared against the conventional method of IDA that uses recorded ground motions. This is done by first obtaining hazard curves for various spectral periods generated using the Campbell and Bozorgnia [38] (CB14) empirical Ground Motion Model (GMM) for each site with the ruptures based on CyberShake-UCERF2 (described in Section 2), using the OpenSHA software [39]. Then the hazard curves are used to develop 15 Uniform Hazard Spectra (UHS) for 15 hazard levels (Return periods of: 5000, 3750, 2500, 1500, 1250, 1000, 900, 700, 500, 300, 200, 100, 75, 50, 25 years). For each UHS at a given site, average S_a ($S_{a_{avg}}^*$) [40] is calculated between the period range of $0.5T^*$ to $2T^*$, where T^* represents the first mode period of each bridge structure. Then for each UHS, 20 recorded ground motions that match the $S_{a_{avg}}^*$ with scaling factors of 0.5–2 are selected. To select the recorded ground motions, a set of 6972 main-shock recordings available in the NGA-West2 database [45] are used. Each ith recorded ground motion ($1 \le i \le 6972$) is scaled with a scaling factor j (in the range $0.5 \le j \le 2$) and its average S_a (${}^jS^i_{a\ avg}$) is computed. ${}^jS^i_{a\ avg}$ is compared against $S_{a_{avg}}^*$ by computing their squared error (${}^jSI = (S^*_{a\ avg} - {}^jS^i_{a\ avg})^2$). Then, for each ith recorded ground motion, the one with the minimum ${}^jSE^i$ is selected, which leads to 6972 scaled ground motions. Among these scaled ground motions, 20 ground motions with minimum ${}^jSE^i$ are selected as a representation of the hazard for the given UHS. This ensures that a ground motion with two different scaling factors is not selected for the same hazard level. Furthermore, once a ground motion is selected for a higher hazard level (higher return period), it is withdrawn from the selection set of 6972 scaled ground motions. In this way, no ground motion is selected more than once across all scaling factors and hazard levels. This process is explained in Fig. 3 and is repeated for all 5 sites and for the 4 bridges to select 20 ground motions for each of the 15 hazard levels. Hence, for each site and each bridge, $20 \times 15 = 300$ unique recorded scaled ground motions are selected. It should be noted that even though the recorded ground motions corresponding to the same hazard level possess similar average S_a, their S_a (T^*) may still differ from each other. The number of ground motions that are classified as pulse-like [29] among the 300 motions for each bridge is given in Table 3. The selected 300 recorded ground motions are used to conduct NLTHA of the four bridge structures and their *Rot50CDR*s are obtained. Hence, a total of 108,000 NLTHA (= 5 sites × 300 ground motions × 4 bridges × 18 intercept angles) are conducted for IDA, i.e., 5,400 NLTHA for each of the four bridges at every site.

4.3. Comparison of simulation-based analysis vs. Incremental Dynamic Analysis

An example of the IM hazard curves and the relation between EDP and IM (denoted as "EDP-IM data") using simulation-based analysis of CyberShake (CS) simulations and *IDA* analysis is presented for Bridge B for the LADT site in Fig. 4. As can be observed from the left side of the figure, the hazard curves obtained from the CyberShake simulations lie in close proximity with the CB14 hazard curve for shorter return periods. For longer return periods (higher hazard levels), the two hazard curves tend to deviate from each other and the results from the CyberShake simulations are lower than the CB14 results. This is noticed for the sites considered; however, it is not a general conclusion for the entire CyberShake site grid.

On the right side of Fig. 4, EDP-IM data from simulation-based

Table 3
Number of pulse-like ground motions among the selected 300 ground motions.

Site	Bridge A	Bridge B	Bridge C	Bridge F
LADT	101	111	97	107
SBSM	144	139	131	135
CCP	108	103	97	100
WNGC	126	124	126	137
STNI	126	113	133	140

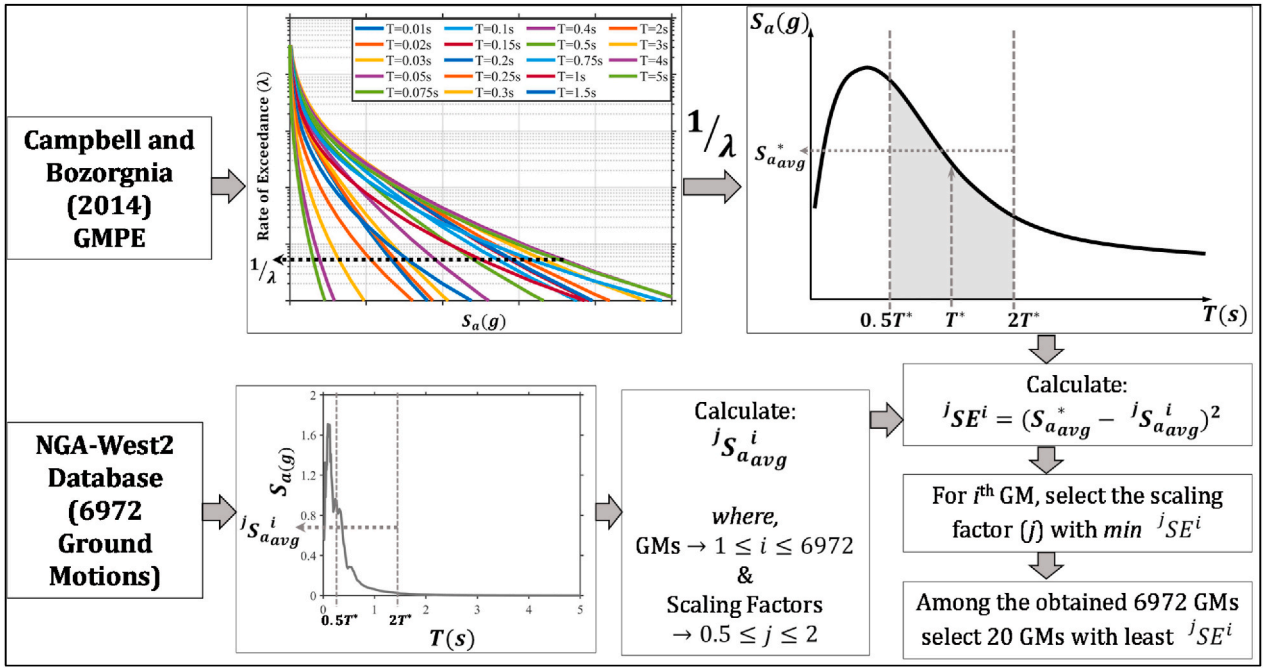

Fig. 3. Illustration of selecting hazard-representative recorded ground motions for IDA.

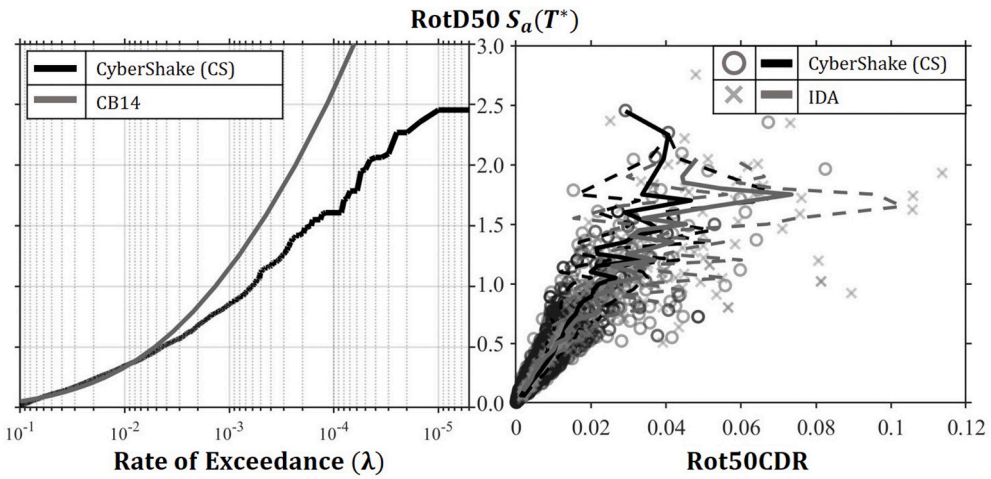

Fig. 4. CyberShake vs. IDA (CB14) for bridge B (T* = 0.8s) at the LADT site.

analysis (CyberShake) tends to show a lower median response for all IM levels and a lower variability for large IM levels as compared to the IDA results. Similar patterns were observed for the other bridges and sites, except for SBSM and STNI, where the variability in EDP-IM data from CyberShake was significantly higher than IDA results. This can be attributed to the fact that the simulated ground motions of these sites include the effects of a deep basin and directivity pulses in terms of intensity, frequency, and duration characteristics. These characteristics

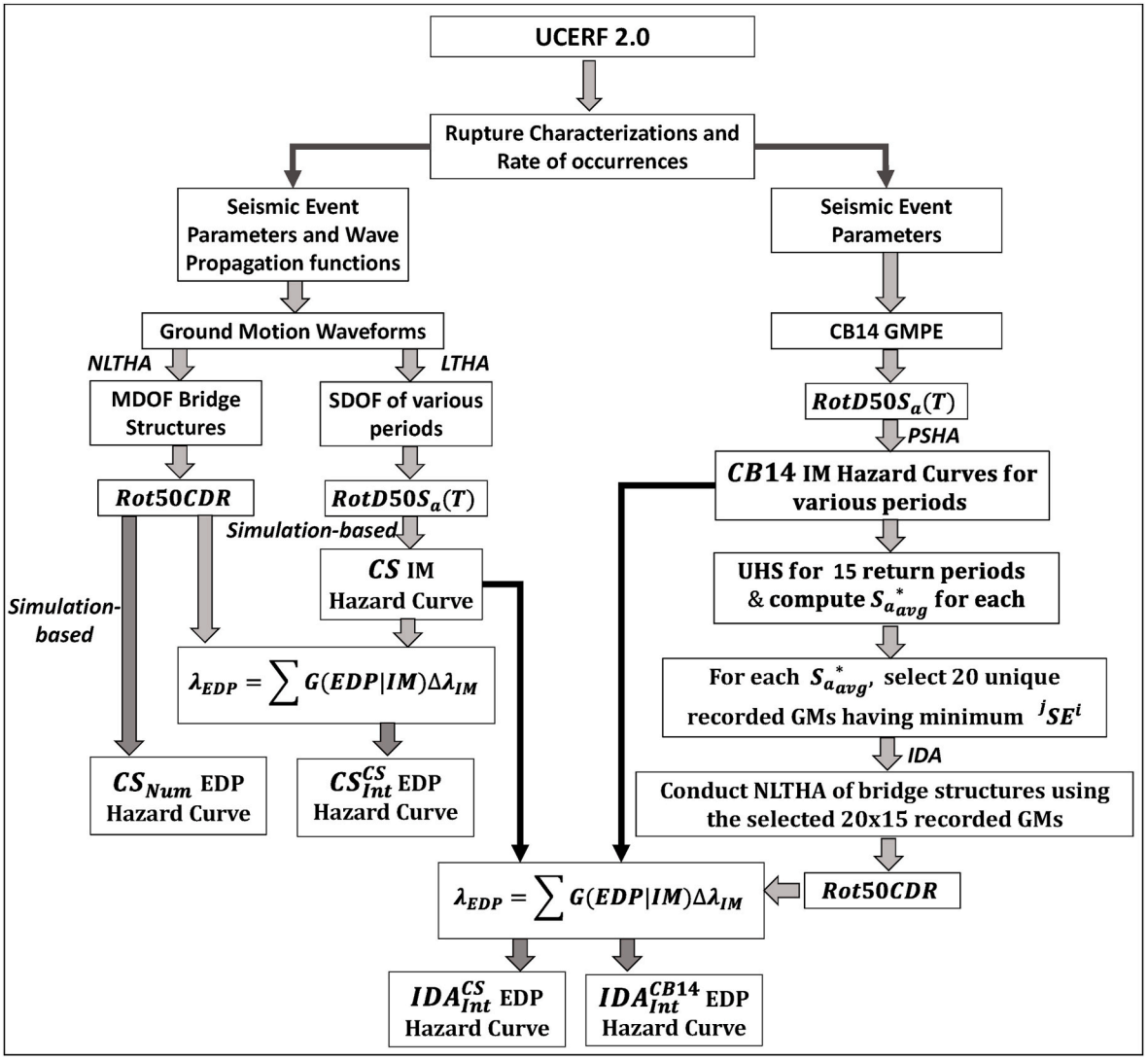

Fig. 5. Illustration of methodology for comparison.

can uniquely affect the response of the bridge structures, causing the variability in EDPs to increase.

The overall methodology of comparison is presented in Fig. 5, where the left side of the figure represents the analysis using simulated ground motions and the right side represents the analysis using recorded ground motions and CB14. Note that both ground motion datasets are based on the rupture characterization from CyberShake-UCERF2. While the IM hazard curves of the simulated ground motions are obtained from Linear-Time-History Analysis (LTHA) of single-degree-of-freedom (SDOF) system for the recorded side, CB14 GMM is used to calculate the IM hazard curves. Furthermore, for the simulated ground motions, two types of EDP hazard curves are obtained using: 1) direct simulations (CS_{num}) and 2) integration (CS_{Int}^{CS}) using Equation (1) [41], where G denotes the survival function, i.e., 1 minus the cumulative distribution function. Similarly, for the recorded ground motions and IDA, two types of EDP hazard curves are calculated by integrating EDP-IM data over: 1) the CB14 IM hazard curve (IDA_{Int}^{CB14}) and 2) the CyberShake IM hazard curve (IDA_{Int}^{CS}). In the next section, comparisons are made between these four EDP hazard curves. In general, the acronyms are defined based on whether the EDP-IM relation used is from recorded motions (denoted by *IDA*) or simulated motions (denoted by *CS*). The subscript defines whether the EDP hazard curve was computed numerically from simulation-based analysis (denoted by *num*) or integration (denoted by *Int*). The superscript defines whether the IM-hazard curve used for integration is based on CB14 (denoted by *CB14*) or CyberShake simulation (denoted by *CS*).

$$\lambda_{EDP} = \sum G(EDP|IM)\Delta\lambda_{IM} \quad (1)$$

5. Results and discussions

5.1. Comparison of IM hazard curves

The comparisons between CyberShake simulations and recorded motions are firstly made by comparing the IM (*RotD50* S_a) hazard curves. This comparison is presented in Fig. 6 in terms of ratios between the *RotD50* S_a obtained from CyberShake (denoted as *RotD*50 Sa_{CS}) and CB14 (denoted as *RotD*50 Sa_{CB14}) for various hazard levels at the five sites. As can be observed from the figures, for all four periods (associated with the four bridges), the hazard curves obtained from CyberShake simulations tend to be closer to those from CB14 for small return periods (<1000 years), with ratios around 0.9, whereas for longer return periods (>1000 years), *RotD*50 Sa_{CB14} tends to be significantly higher than *RotD*50 Sa_{CS}, thereby leading to ratios close to 0.6. Particularly at sites STNI and WNGC, it is observed that *RotD*50 Sa_{CS} is significantly smaller than *RotD*50 Sa_{CB14} across all hazard levels. Also, across all the sites, it is observed that hazard curves from CB14 and CyberShake simulations differ most for $T = 1.1$ s (Bridge F). In general, it is observed that near the return period of 975 years, the two hazard curves have a ratio of ~0.85. This hazard level is vital for bridge engineers because bridges are designed for seismic demands associated with a return period of 975 years [32]. In summary, from Fig. 6, it can be deduced that the IM hazard curves arising from CB14 and CyberShake simulations differ from each other; the differences mainly lie towards the longer return periods where CB14 tends to estimate higher *RotD50* S_a than CyberShake simulations. Such differences are consistent with observations made by other studies (such as [42]. Since typical GMMs are fitted to global data, they may lead to the overestimation or underestimation of *RotD50* S_a compared to simulations that represent regional characteristics.

5.2. Comparison of EDP hazard curves

Fig. 7 presents the four types of EDP hazard curves defined above in Fig. 5, for the four bridges and the LADT site. Recall that the EDP hazard curves obtained from simulation-based analysis of CyberShake simulations are termed CS_{num}, while the EDP hazard curves obtained by integrating the CB14 IM hazard curves with EDP-IM (i.e., IDA) data are denoted as IDA_{Int}^{CB14}. Though the two types of EDP hazards are compared to contrast the simulated results from the recorded ones, the differences between the two types can also be attributed to other factors. Computation of IDA_{Int}^{CB14} involves integration over an IM; computation of CS_{num}

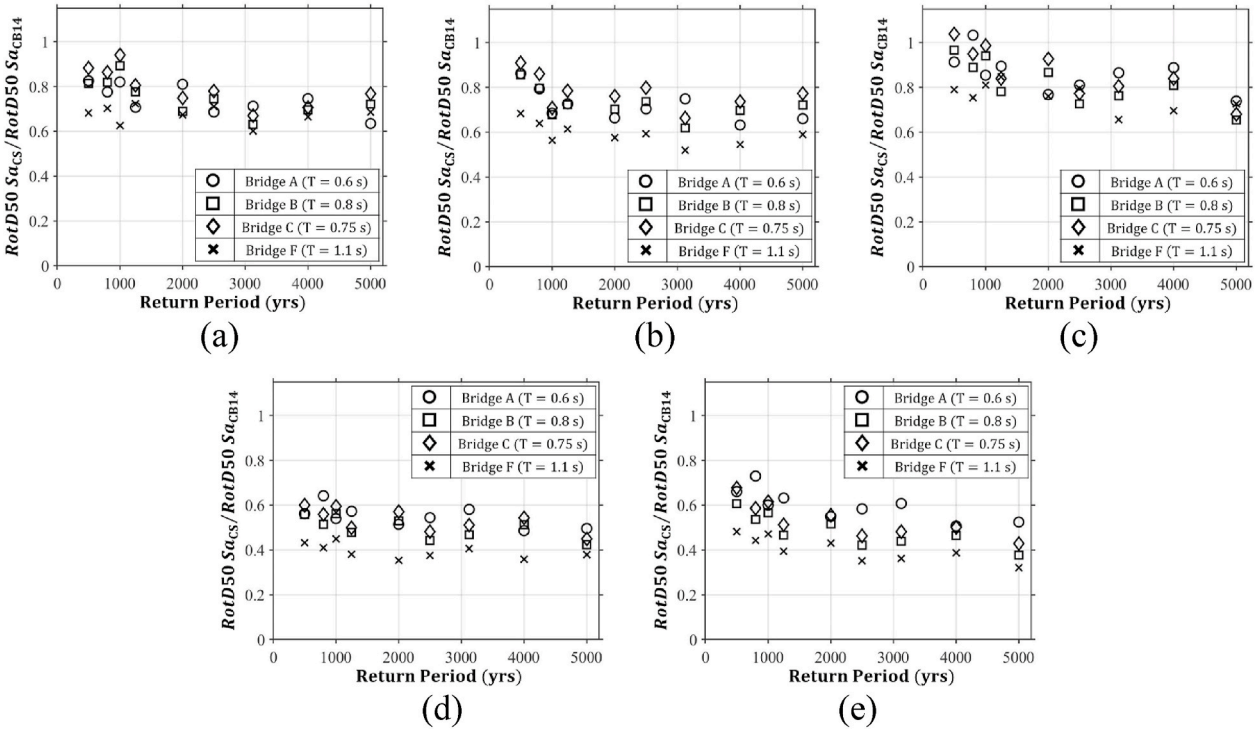

Fig. 6. Ratio of *RotD*50 Sa_{CS}/*RotD*50 Sa_{CB14} *vs.* return period (hazard level) for: (a) CCP, (b) LADT, (c) SBSM, (d) STNI, and (e) WNGC.

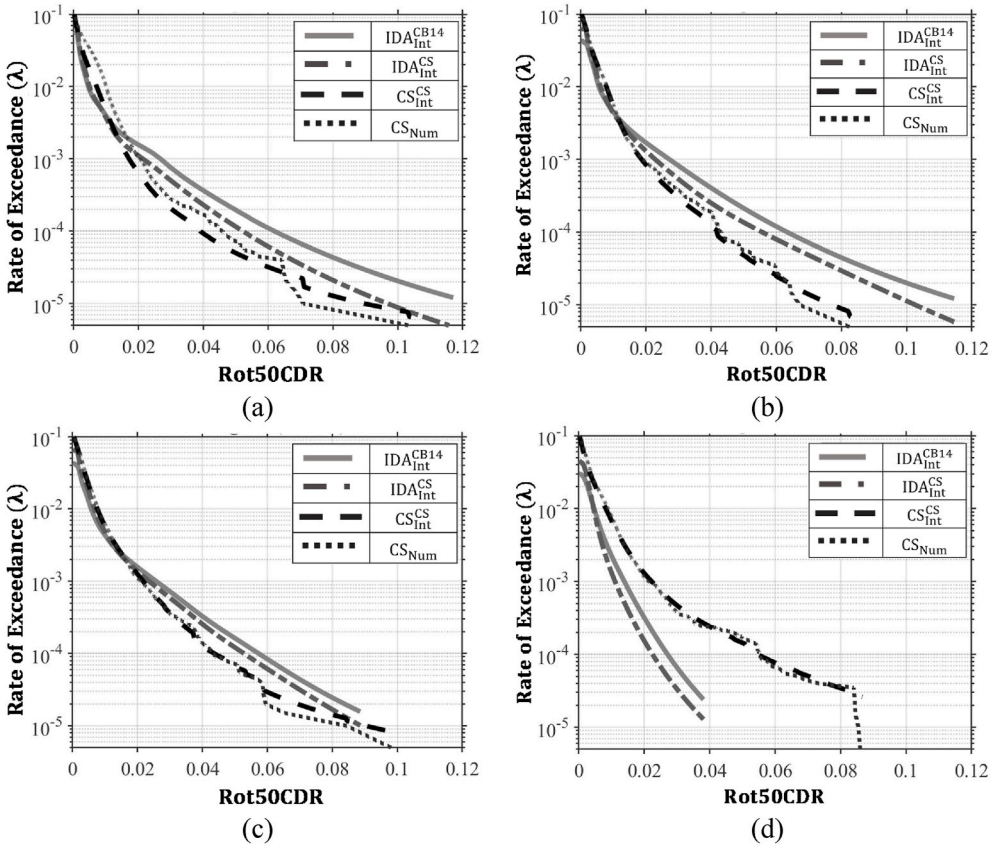

Fig. 7. *Rot50CDR* (EDP) hazard curves for LADT site bridges: (a) A, (b) B, (c) C, and (d) F.

is direct and does not include any such integration. Numeric integration is primarily based on discretization and summation and hence can lead to an inherent bias. Also, it is important to differentiate the differences in EDP hazard curves arising from differences in IM hazard curves or EDP-IM data. To do so, two other types of EDP hazard curves are introduced. To incorporate integration in the data obtained from simulation-based analysis of CyberShake simulations, the IM hazard curves obtained from CyberShake simulations are integrated over the CyberShake EDP-IM data of each site for each bridge, using Equation 1. The EDP hazard curves generated from this integration are termed CS_{Int}^{CS}. Note that the data sizes used to develop CS_{Int}^{CS} and IDA_{Int}^{CB14} are different. CS_{Int}^{CS} is developed using ~20,000 ground motions while IDA_{Int}^{CB14} is obtained using 300 ground motions (due to limitation of useable recorded ground motions). The latter may impact the computation of $G(EDP|IM)$ due to lower number of ground motions; however from Fig. 4, it can be observed that the influence of this dicrepancy is not large for ground motions with $S_a < 1.5$ g (it mainly leads to a lesser number of ground motions for large S_a levels). Furthermore, to account for the differences in EDP hazard curves due to differences in IM hazard curves, the CyberShake IM hazard curve is also integrated over the EDP-IM data of the IDA analysis. The EDP hazard curves obtained from this integration are denoted IDA_{Int}^{CS}.

Since both IDA_{Int}^{CB14} and IDA_{Int}^{CS} use the EDP-IM data of recorded IDA analysis, the difference between the two EDP hazard curves is primarily due to the differences between the CB14 and CS IM hazard curves. This shows the sensitivity of the EDP hazard curves to differences in the IM hazard curves (i.e., CB14 vs. CyberShake). Similarly, the EDP hazard curves CS_{Int}^{CS} and IDA_{Int}^{CS} are developed using the IM hazard curve obtained from CyberShake data; however, their differences are attributed to the EDP-IM data. A comparison between the three EDP hazard curves shows that the differences between IDA_{Int}^{CB14} and CS_{Int}^{CS} can be mostly attributed to the differences between the EDP-IM characteristics rather than the IM hazard curves. Fig. 7 shows that CS_{num} and CS_{Int}^{CS} EDP hazard curves lie very close to each other for all bridges, demonstrating that the integration does not introduce significant differences. This means either CS_{num} or CS_{Int}^{CS} can be used for comparison with other EDP hazard curves, and the results are equally viable for both EDP hazard curves.

It is observed from Fig. 7 that, for bridges with shorter return periods (A, B, and C), IDA_{Int}^{CB14} lies in the vicinity of CS_{num} for smaller return periods; for longer return periods, IDA_{Int}^{CB14} consistently leads to higher values of *Rot50CDR* as compared to CS_{num}. For Bridge F, it is observed that CS_{num} leads to higher *Rot50CDR* as compared to IDA_{Int}^{CB14} for all hazard levels. As mentioned in the Ground Motion Database section (Section 2), CyberShake 15.12 simulations are a hybrid of deterministic and stochastic simulations; the higher frequency content (>1 Hz) is simulated with stochastic approaches and is added to the physics-based deterministic ground motion time series corresponding to lower frequency content (≤1 Hz). This could explain why the CyberShake ground motions affect the response differently than the recorded motions for the bridges with shorter periods (Bridges A, B, and C) as compared to the bridges with longer periods (Bridge F). Since the selected recorded ground motions do not specifically belong to the southern California basin and hence do not explicitly account for the local site-, basin-, and directivity-effects, the IDA_{Int}^{CB14} tends to be similar for bridges A, B, C, and F. This is consistent with the findings of Bijelić et al. [25]; who used building structures to compare simulation-based EDP hazard curves with conventional methods.

As mentioned earlier, to understand whether the differences in EDP hazard curves arise from the differences in IM hazard curves or EDP-IM data, IDA_{Int}^{CB14} is compared against IDA_{Int}^{CS} and CS_{Int}^{CS}. As illustrated in all sub-figures of Fig. 7, IDA_{Int}^{CS} tends to be lower than IDA_{Int}^{CB14} across all hazard levels. This can be attributed to the fact that the IM hazard curve obtained from CyberShake tends to be lower than the IM hazard curve

from CB14. Hence the integration process of Equation (1) accumulates the differences in the IM hazard curve, leading to larger differences in the EDP hazard curves, especially for higher hazard levels. However, it can be observed that the differences between the two EDP hazard curves (IDA_{Int}^{CB14} and IDA_{Int}^{CS}) do not significantly account for differences between CS_{Int}^{CS} (or CS_{num}) and IDA_{Int}^{CB14}, which represents the differences between simulations and IDA. It is concluded that the differences in IM hazard curves do not sufficiently account for the differences in EDP hazard curves.

The comparison of IDA_{Int}^{CS} against CS_{Int}^{CS} describes the significance of differences in EDP-IM data leading to differences in EDP hazard curves. It can be observed from Fig. 7 that CS_{Int}^{CS} and IDA_{Int}^{CS} for all the bridge structures are significantly different from each other, with CS_{Int}^{CS} corresponding to lower *Rot50CDR* across all hazard levels for the bridges with shorter periods (A, B, and C). For the longer period bridge (Bridge F), the differences in the CS_{Int}^{CS} and IDA_{Int}^{CS} are observed to be much higher than CS_{Int}^{CS} and IDA_{Int}^{CB14} since the use of the CyberShake IM hazard curve for integration further decreases the EDP hazard curve. Hence, it can be deduced that the primary differences in the EDP hazard curves arise from the differences in the EDP-IM data, and IM hazard curves are not sufficiently capable of describing changes in EDP hazard curves for bridge structures. This can be primarily due to the fact that $G(EDP|IM)$ bears larger weight in the integration process, and differences in the probabilities of EDP|IM causes major shifts in the EDP hazard curves. The statistical moments of $G(EDP|IM)$ can significantly change and lead to major differences in the integration process depending on the number of data points used to build the function. Similar trends were observed for the other four sites included in this study, and the differences were observed to be larger for the sites having higher basin and directivity effects (SBSM and STNI). Accordingly, it is recommended that the engineering community should validate simulated ground motions not only based on IM levels but also based on more in-depth comparisons made on the EDP-IM level.

6. Dependencies of differences in EDP hazard curves on hazard level and site parameters

To further understand the reasons and parameters that affect the differences between EDPs obtained from simulated and recorded motions, here the focus is directed towards ratios of EDPs (*Rot50CDR*) and IMs (*RotD50* S_a) obtained from the two methods. Fig. 8 shows the ratios of various EDPs from the four EDP hazard curves (CS_{Int}^{CS}, IDA_{Int}^{CS}, IDA_{Int}^{CB14} and CS_{num}). Furthermore, these ratios are regressed on hazard level (in years), and site characteristics V_{s30} (in m/s) and $Z_{2.5}$ (in m).

Fig. 8 presents the relationship between the ratio of $Rot50CDR_x$ (EDP) and $Rot50CDR_y$ (EDP), where x and y denote the EDPs obtained from the four types of EDP hazard curves (CS_{Int}^{CS}, IDA_{Int}^{CS}, IDA_{Int}^{CB14}, and CS_{num}). As a general observation, it can be seen that the ratios for Bridges A, B, and C tend to vary slightly with the return period, whereas for Bridge F an increasing trend is observed. The ratios of $Rot50CDR_{IDA_{Int}^{CB14}}$ and $Rot50CDR_{IDA_{Int}^{CS}}$ tend to be slightly higher than 1, which shows that differences in the IM hazard curves do not significantly change the EDP hazard curves, but IDA_{Int}^{CB14} continues to lead to higher values as compared to IDA_{Int}^{CS}. Moreover, the ratios between $Rot50CDR_{CS_{num}}$ and $Rot50CDR_{CS_{Int}^{CS}}$ are very close to 1, which portrays little effect from the integration involved in computing EDP hazard curves. Ratios of $Rot50CDR_{CS_{num}}$ to $Rot50CDR_{IDA_{Int}^{CB14}}$ and $Rot50CDR_{CS_{Int}^{CS}}$ to $Rot50CDR_{IDA_{Int}^{CB14}}$ lead to values of ~0.6 for Bridges A, B, and C, and ~1.6 for Bridge F. This means, in general, there is a ~40% reduction in *Rot50CDR* arising from simulation-based analysis of CyberShake 15.12 simulations as compared to IDA using recorded ground motions for the shorter period bridges. For the bridge with a longer period, Bridge F, a ~60%–~70% increase in *Rot50CDR* arises from the simulation-based analysis. Lastly, the ratios of $Rot50CDR_{CS_{Int}^{CS}}$ and $Rot50CDR_{IDA_{Int}^{CS}}$ lie very close to 0.75 for Bridges A, B,

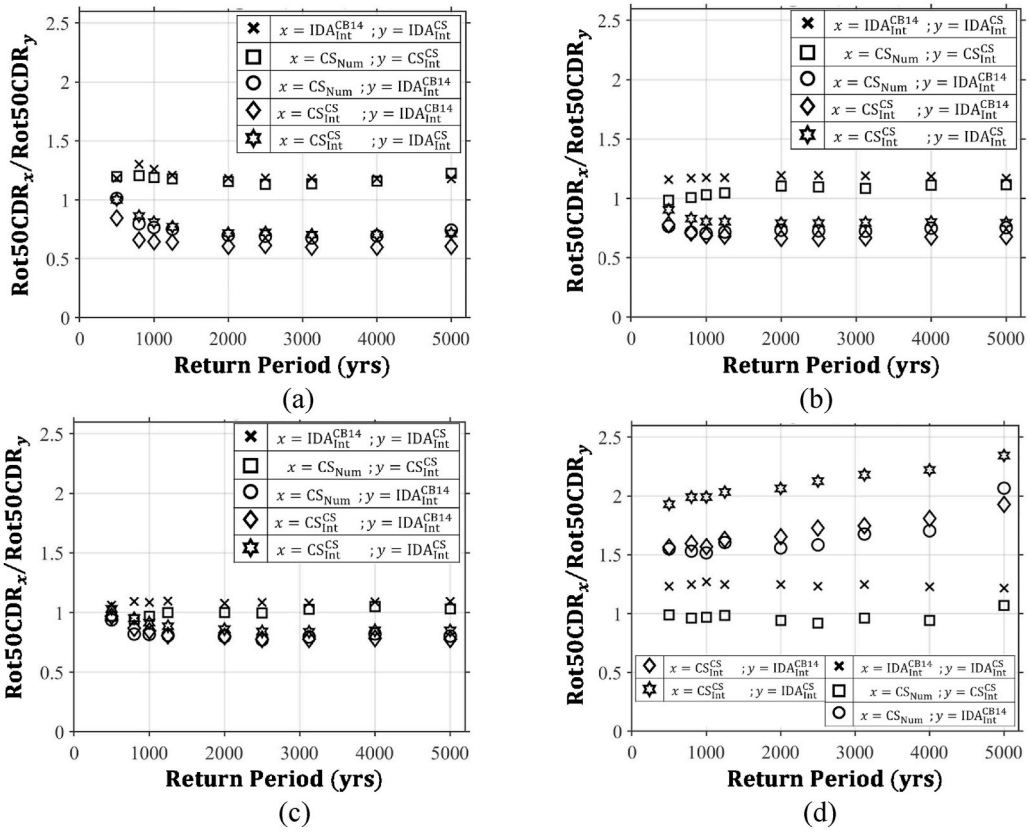

Fig. 8. Ratio of $Rot50CDR_x$ (EDP) and $Rot50CDR_y$ (EDP) *vs* return period (hazard level) for LADT site for bridges: (a) A, (b) B, (c) C, and (d) F.

and C and close to 2 for Bridge F. This means that the majority of the differences in EDP hazard curves using the CyberShake simulations and record-based IDA method arise from the differences in the EDP-IM data. Similar patterns were noticed for other sites with certain exceptions in the values of the ratios.

To assist with improving ground motion simulation methods using this research (or similar research where probabilistic seismic demand analysis is used for validation of a ground motion simulation method), dependencies of the difference in the response of each type of bridge (A, B, C, and F) on return period and site parameters are provided. This is done by combining the results from all sites and conducting mixed-effects regression analysis with the target variable being the ratio of EDPs from simulation-based analysis of CyberShake simulations ($Rot50CDR_{CS_{num}}$) and from IDA using CB14 ($Rot50CDR_{IDA_{Int}^{CB14}}$). The predictor variables include return period (RP), V_{s30}, and $Z_{2.5}$. This is expressed in Equation (2) and is fitted to data independently for each bridge. In Equation (2), ε_{ij} represents the within-site variability for the ith hazard level and jth site with zero mean and variance of φ^2, and σ_i represents the between-site variability for the ith hazard level with zero mean and variance of τ^2. The coefficients and the goodness-of-fit measure (R^2_{adj}) for each bridge are given in Table 4.

$$\ln\left(\frac{Rot50CDR_{CS_{num}}}{Rot50CDR_{IDA_{Int}^{CB14}}}\right)=b_0+b_1(\ln(RP))+b_2(\ln(V_{s30}))+b_3(\ln(Z_{2.5}))+\varepsilon_{ij}\left(0,\varphi^2\right)+\sigma_i\left(0,\tau^2\right) \quad (2)$$

It can be observed from Table 4 that for all four bridges the value of φ is higher than τ, which means that the within-site variability is highly explanatory in the computation of the EDP ratio $Rot50CDR_{CS_{num}}/Rot50CDR_{IDA_{Int}^{CB14}}$. Also, the goodness-of-fit measure R^2_{adj} is observed to be consistently above 0.95, which means that the regression equations can estimate the EDP ratios for the four bridge structures with a high level of accuracy. The coefficient b_1 is observed to be negative for bridges A, B, and C, demonstrating that as the return period increases, $Rot50CDR_{IDA_{Int}^{CB14}}$ tends to be larger than $Rot50CDR_{CS_{num}}$; the opposite is the case for bridge F. This is due to the higher variability in EDPs in EDP-IM data caused by recorded ground motions, especially for larger IM levels. This can be observed from Fig. 5 especially for ground motions with $S_a > 1.5$ g. The integration process accumulates this variability, causing the EDP hazard curve $Rot50CDR_{IDA_{Int}^{CB14}}$ to grow faster as compared to $Rot50CDR_{CS_{num}}$. The value of b_2 is positive for all four bridges, with the highest value being noted for bridge F. This means that with an increase in V_{s30} of the site, $Rot50CDR_{CS_{num}}$ tends to increase as compared to $Rot50CDR_{IDA_{Int}^{CB14}}$. This effect is observed to be highly dominant for Bridge F that has a longer period than the other OSBs. Furthermore, the coefficient b_3 is negative for shorter-period bridges A, B, and C, while it is significantly positive for Bridge F. This trend shows that with an increase in basin depth $Z_{2.5}$, $Rot50CDR_{CS_{num}}$ tends to be lower than $Rot50CDR_{IDA_{Int}^{CB14}}$ for shorter-period bridges (A, B, and C). For the longer-period Bridge F, it is observed that a deeper basin tends to increase the EDP ratio and leads to higher $Rot50CDR_{CS_{num}}$ as compared to $Rot50CDR_{IDA_{Int}^{CB14}}$. This is postulated to be due to the fact that the simulated ground motions, specifically for the sites with significant basin effects (SBSM and STNI), possess high basin and directivity effects, which alters the lower frequency content of the ground motions. This alteration in lower frequencies tends to increase the variability in EDP-IM of Bridge F (possessing longer natural period), which leads to an increase in the $Rot50CDR_{CS_{num}}$ EDP hazard curve. However, the impact of these basin effects is not observed to be highly prominent in the EDP-IM relationship for the shorter-period bridges A, B, and C. The stochastic part (frequency content > 1 Hz) of the CyberShake simulated ground motions is modeled using a plane-layer velocity structure and the basin effects are captured approximately via the V_{s30} amplification factors. These features may be responsible for significantly different behavior observed for the regressions of Bridges A, B, and C versus Bridge F. In general, for bridge analysis, it is concluded that there is a need for detailed site-specific analysis because basin effects and site amplification can lead to significant changes in the response of bridge structures. The relations provided in Table 4 can assist engineers in validating their methods of bridge analysis and can be used in scaling the EDPs as per the design site. It should be noted that the regression equations proposed in this study are based on the CyberShake 15.12 simulations of five southern California sites with soft soils; hence, they can be biased towards these conditions. However, these equations can provide initial estimates of the scaling factors and can be easily updated with more data from different site conditions.

Table 4
Fitted coefficients of the mixed-effects regression.

Bridge	b_0	b_1	b_2	b_3	φ	τ	R^2_{adj}
A	−11.169	−0.142	2.124	−0.269	0.261	0.094	0.96
B	−15.781	−0.076	2.799	−0.291	0.162	0.069	0.97
C	−14.371	−0.055	2.516	−0.241	0.139	0.063	0.97
F	−40.165	0.017	6.844	0.427	0.207	0.093	0.98

7. Conclusions

The study presented herein evaluates simulated ground motions using probabilistic seismic demand analysis. The evaluation is of CyberShake (ver 15.12) simulations for an application in the engineering of Ordinary Standard Bridges (OSBs). Catalogs of simulated ground motions representing a time-span of 200,000 years for five sites in southern California with diverse site and local seismicity conditions are obtained from CyberShake (i.e., 20,000 ground motions from events with $M_w > 6.0$ occurring within 200 km of each site) and applied to four OSB structures. In parallel, a set of hazard-targetted scaled recorded ground motions are used to conduct Incremental Dynamic Analysis (IDA) of the four bridge structures (to build EDP-IM relations) that are integrated with the ground motion Intensity Measure (IM) hazard curves to attain EDP hazard curves. NLTHA is conducted to calculate the bridge Column Drift Ratio (CDR); the effect of uncertainty in the ground motion incidence angle is incorporated by rotating the applied time-series at 10° increments. The evaluation is composed of two components: (1) estimates of Engineering Demand Parameters (EDP) at various return periods are compared from EDP hazard curves obtained from NonLinear Time-History Analysis (NLTHA) using simulated and recorded motions; and (2) sources of the differences between the two types of EDP hazard curves are identified, namely differences in IM hazard curves or differences in the EDP-IM relation obtained from simulated and recorded motions. Unlike validation studies that are primarily based on ground motion intensity measures, this validation study uses NLTHA of bridge models. The evaluation is done on five CyberShake sites to make comparisons between the CyberShake 15.12 study and conventional record-based IDA.

The results show that using the CyberShake (ver. 15.12) simulation study is relatively similar to using recorded ground motions for seismic

performance assessment of OSBs with shorter periods. For the OSB with longer period ($T = 1.1$ s), the EDPs obtained from simulation-based analysis tend to be higher than the EDPs obtained from utilizing recorded ground motions. Further observations suggest that the difference between EDP-IM data is the primary source of EDP hazard curve variations. To account for site-specific differences in the EDP hazard curves obtained from simulation-based analysis, dependencies are provided using regression. The regression equations relate the ratio between the EDPs obtained from simulation-based analysis and record-based IDA with the hazard return period and site characteristics V_{s30} and $Z_{2.5}$. It is recommended that validation efforts go beyond comparisons of IM levels and also include EDP-IM level validation. Especially for long-period bridge structures, further analysis is recommended to compare the EDP-IM obtained from CyberShake with those of recorded motions. Note that the results and analysis presented in this study only pertain to CyberShake 15.12 study and the methodology used to select recorded ground motions for IDA. Other CyberShake studies coupled with different selection procedures for recorded ground motions may lead to different conclusions. However, the methodology used here can be easily extended to other simulation studies and other types of structures.

Author statement

Jawad Fayaz: Methodology, Investigation, Writing - Original Draft, Software; ***Sanaz Rezaeian*:** Conceptualization, Editing, ***Farzin Zareian***: Conceptualization, Methodology, Writing - Review & Editing, Supervision.

Declaration of competing interest

The authors declare that they have no known competing financial interests or personal relationships that could have appeared to influence the work reported in this paper.

Acknowledgments

This research was supported by the the Southern California Earthquake Center (SCEC) with funding from the NSF and U.S. Geological Survey. Their support is gratefully acknowledged. Any use of trade, firm, or product names is for descriptive purposes only and does not imply endorsement by the U.S. Government. The authors thank Dr. Robert Graves and Dr. Nicolas Luco for providing reviews on the results and conclusions of this study.

Appendix A. Supplementary data

Supplementary data to this article can be found online at https://doi.org/10.1016/j.soildyn.2020.106533.

References

[1] Nist. Selecting and scaling earthquake ground motions for performing response-history analyses. 2011. p. 256. NIST GCR 11-917-15 (ATC 82), prepared by the *NEHRP Consultants Joint Venture for the* National Institute of Standards and Technology. Gaithersburg, MD, USA.
[2] Asce 7-05. Minimum design loads for buildings and other structures. Reston, VA: American Society of Civil Engineers/Structural Engineering Institute; 2005. ASCE 7-05.
[3] Tbi. Guidelines for performance-based seismic design of Tall buildings. Version 2.03. Developed by the *pacific earthquake engineering research center* (PEER) as part of the Tall building initiatives (TBI). 2017. p. 147. PEER Report No. 2017/06.
[4] Asce 7-16. Minimum design loads for buildings and other structures. Reston, VA: American Society of Civil Engineers/Structural Engineering Institute; 2017. ASCE 7-16.
[5] Luco N, Bazzurro P. Does amplitude scaling of ground motion records result in biased nonlinear structural drift responses? Earthq Eng Struct Dynam 2007;36(13):1813–35.
[6] Haselton CB, Whittaker AS, Hortacsu A, Baker JW, Bray J, Grant DN. Selecting and scaling earthquake ground motions for performing response-history analyses. In: Proceedings of the 15th world conference on earthquake engineering; 2012. p. 4207–17.
[7] Rezaeian S, Zhong P, Hartzell S, Zareian F. Validation of simulated earthquake ground motions based on evolution of intensity and frequency content. Bull Seismol Soc Am 2015;105(6):3036–49.
[8] Atkinson GM, Assatourians K. Implementation and validation of EXSIM (a stochastic finite-fault ground-motion simulation algorithm) on the SCEC Broadband platform. Seismol Res Lett 2014;86(1):48–60.
[9] Boore DM. Comparing stochastic point-source and finite-source ground-motion simulations: SMSIM and EXSIM. Bull Seismol Soc Am 2009;99(6):3202–16.
[10] Graves R, Pitarka A. Refinements to the Graves and Pitarka (2010) Broadband ground-motion simulation method. Seismol Res Lett 2015;86:75–80.
[11] Song SG, Somerville P. Physics-based earthquake source characterization and modeling with geostatistics. Bull Seismol Soc Am 2010;100(2):482–96.
[12] Star L, Stewart J, Graves R. Comparison of ground motions from hybrid simulations to NGA prediction equations. Earthq Spectra 2011;27:331–50. https://doi.org/10.1193/1.3583644.
[13] Galasso C, Zhong P, Zareian I, Graves R. Validation of ground motion simulations for historical events using MDoF systems. Earthq Eng Struct Dynam 2013;42(9):1395–412.
[14] Galasso C, Kaviani P, Tsioulou A, Zareian F. Validation of ground motion simulations for historical events using skewed bridges. J Earthq Eng 2018:1–23.
[15] Burks LS, Baker JW. Validation of ground motion simulations through simple proxies for the response of engineered systems. Bull Seismol Soc Am 2014;104(4):1930–46.
[16] Goulet CA, Abrahamson NA, Somerville PG, Wooddell KE. The SCEC Broadband platform validation exercise: methodology for code validation in the context of seismic-hazard analyses. Seismol Res Lett 2015;86(1):17–26.
[17] Zhong P. Ground Motion Simulation Validation for building design and response assessment. Irvine, CA: University of California – Irvine; 2016. Ph.D. Dissertation.
[18] Bradley B, Pettinga D, Baker JF, Fraser J. Guidance on the utilization of earthquake-induced ground motion simulations in engineering practice. Earthq Spectra 2017;33(3):809–35.
[19] Tsioulou A, Taflanidis AA, Galasso C. Validation of stochastic ground motion model modification by comparison to seismic demand of recorded ground motions. Bull Earthq Eng 2019;17(6):2871–98.
[20] Naeim F, Graves RW. The case for seismic superiority of well-engineered tall buildings. Struct Des Tall Special Build 2006;14:401–16.
[21] Jones P, Zareian F. Relative safety of high-rise and low-rise steel moment-resisting frames in Los Angeles. Struct Des Tall Special Build 2010;19:183–96.
[22] Yoon YH, Ataya S, Mahan M, Malek A, Saiidi MS, Zokaie T. Probabilistic damage control application: implementation of performance-based earthquake engineering in seismic design of highway bridge columns. J Bridge Eng 2019;24(7):04019068. 2019.
[23] Fayaz J, Dabaghi M, Zareian F. Utilization of site-based simulated ground motions for hazard-targeted seismic demand estimation: application for ordinary bridges in southern California. J Bridge Eng 2020;25(11):04020097.
[24] Latbsdc. An alternative procedure for seismic analysis and design of Tall buildings located in the Los Angeles region. 2020 Edition 2020 [A consensus document developed by the Los Angeles Tall Buildings Structural Design Council (LATBSDC)].
[25] Bijelić N, Lin T, Deierlein GG. Evaluation of building collapse risk and drift demands by nonlinear structural analyses using conventional hazard analysis versus direct simulation with CyberShake seismograms. Bull Seismol Soc Am 2019;109(5):1812–28.
[26] Graves R, Jordan TH, Callaghan S, et al. CyberShake: a physics-based seismic hazard model for southern California. Pure Appl Geophys 2011;168(3):367–81.
[27] Field EH, Dawson TE, Felzer KR, Frankel AD, Gupta V, Jordan TH, Wills CJ. Uniform California earthquake rupture forecast, version 2 (UCERF 2). Bull Seismol Soc Am 2009;99(4):2053–107.
[28] Lee EJ, Chen P, Jordan TH, Maechling PB, Denolle MAM, Beroza GC. Full-3-D tomography for crustal structure in Southern California based on the scattering-integral and the adjoint-wavefield methods. J. Geophys. Res. Solid Earth 2014;119:6421–51.
[29] Shahi SK, Baker JW. An efficient algorithm to identify strong-velocity pulses in multicomponent ground motions. Bull Seismol Soc Am 2014;104(5):2456–66.
[30] McKenna F, Scott MH, Fenves GL. Nonlinear finite element analysis software architecture using object composition. J Comput Civ Eng 2010;24(1):95–107.
[31] Caltrans. Seismic design Criteria. California Department of Transportation; 2013. Version 1.7.
[32] Caltrans. Seismic design Criteria. California Department of Transportation; 2019. Version 2.0.
[33] Kottari A. Design and capacity assessment of external shear keys in bridge abutments. San Diego: Department of Structural Engineering, University of California; 2016. Ph.D. Thesis.
[34] Choi E. Seismic analysis and retrofit of mid-America bridges. Atlanta (G.A.): Department of Civil and Environmental Engineering, Georgia Institute of Technology; 2002. Ph.D. Thesis.
[35] Shamsabadi A, Kapuskar M. Nonlinear seismic soil-abutment-structure interaction analysis of skewed bridges. In: Proc 5th national seismic conference on bridges and highways; 2006.
[36] Ramanathan K. Next generation seismic fragility curves for California bridges incorporating the evolution in Seismic design philosophy. Atlanta (G.A.): Department of Civil and Environmental Engineering, Georgia Institute of Technology; 2012. Ph.D. Thesis.

[37] Boore DM. Orientation-independent, nongeometric-mean measures of seismic intensity from two horizontal components of motion. Bull Seismol Soc Am 2010; 100:1830–5.
[38] Campbell KW, Bozorgnia Y. Campbell-Bozorgnia NGA-West2 horizontal ground motion model for active tectonic domains. Earthq Spectra 2014;30(3):1087–115.
[39] Field EH, Jordan TH, Cornell CA. OpenSHA: a developing community-modeling environment for seismic hazard analysis. Seismol Res Lett 2003;74(4):406–19.
[40] Eads L, Miranda E, Lignos DG. Average spectral acceleration as an intensity measure for collapse risk assessment 2015;44(12):2057–73.
[41] Cornell CA, Jalayer F, Hamburger RO, Foutch D. Probabilistic basis for 2000 SAC Federal Emergency Management Agency steel moment frame guidelines. J Struct Eng 2002;128(4):526–33.
[42] Teng G, Baker J. Evaluation of SCEC CyberShake ground motions for engineering practice. Earthq Spectra 2019;35(3):1311–28.
[44] Galasso, C., Zareian, F., Iervolino, I., Graves, R. W. Validation of ground motion simulations for historical events using SDOF systems. Bull Seismol Soc Am, 2012, 102(6), 2727-2740. 0037-1106.
[45] Timothy DA, Robert BD, Jonathan PS, Emel S, Walter JS, Brian S, Chiou J, Wooddell KE, Graves RW, Kottke AR, Boore DM, Kishida T, Donahue JL. NGA-West2 database. Earthq Spectra 2014;30(3):989–1005.
[46] Maechling PJ, Silva F, Callaghan S, Jordan TH. SCEC broadband platform: System architecture and software implementation. Seismol Res Lett 2015;86:27–38. https://doi.org/10.1785/0220140125. January/February 2015.